microLife, 2024, **5**, uqae014
DOI: 10.1093/femsml/uqae014
Advance access publication date: 12 June 2024
Research Article

Coordinated regulation of osmotic imbalance by c-di-AMP shapes ß-lactam tolerance in Group B *Streptococcus*

Terry Brissac[1], Cécile Guyonnet[2,3,4], Aymane Sadouni[1], Ariadna Hernández-Montoya[1], Elise Jacquemet[5], Rachel Legendre[5], Odile Sismeiro[1], Patrick Trieu-Cuot[1], Philippe Lanotte[6,7], Asmaa Tazi[2,3,4], Arnaud Firon [1,*]

[1]Department of Microbiology, Biology of Gram-positive Pathogens, Institut Pasteur, Université Paris Cité, 75015, Paris, France
[2]Université Paris Cité, Institut Cochin, Institut National de la Santé et de la Recherche Médicale U1016, Centre National de la Recherche Scientifique UMR8104, Team Bacteria and Perinatality, 75015, Paris, France
[3]Department of Bacteriology, French National Reference Center for Streptococci, Assistance Publique-Hôpitaux de Paris Hôpitaux Universitaires Paris Centre, Hôpital Cochin, 75005, Paris, France
[4]Fédération Hospitalo-Universitaire Fighting Prematurity,75005, Paris, France
[5]Institut Pasteur, Université Paris Cité, Bioinformatics and Biostatistics Hub, 75015 Paris, France
[6]Université de Tours, INRAE, UMR 1282 ISP, 3700, Tours, France
[7]CHRU de Tours, Service de Bactériologie-Virologie, 37044, Tours, France
*Corresponding author. Department of Microbiology, Institut Pasteur, 25–28 rue du Docteur Roux, 75724 Paris Cedex 15, Paris, France. E-mail: arnaud.firon@pasteur.fr
Editor: [Carmen Buchrieser]

Abstract

Streptococcus agalactiae is among the few pathogens that have not developed resistance to ß-lactam antibiotics despite decades of clinical use. The molecular basis of this long-lasting susceptibility has not been investigated, and it is not known whether specific mechanisms constrain the emergence of resistance. In this study, we first report ß-lactam tolerance due to the inactivation of the c-di-AMP phosphodiesterase GdpP. Mechanistically, tolerance depends on antagonistic regulation by the repressor BusR, which is activated by c-di-AMP and negatively regulates ß-lactam susceptibility through the BusAB osmolyte transporter and the AmaP/Asp23/GlsB cell envelope stress complex. The BusR transcriptional response is synergistic with the simultaneous allosteric inhibition of potassium and osmolyte transporters by c-di-AMP, which individually contribute to low-level ß-lactam tolerance. Genome-wide transposon mutagenesis confirms the role of GdpP and highlights functional interactions between a lysozyme-like hydrolase, the KhpAB RNA chaperone and the protein S immunomodulator in the response of GBS to ß-lactam. Overall, we demonstrate that c-di-AMP acts as a turgor pressure rheostat, coordinating an integrated response at the transcriptional and post-translational levels to cell wall weakening caused by ß-lactam activity, and reveal additional mechanisms that could foster resistance.

Keywords: nucleotide signaling; osmolytes; turgor pressure; cell wall; antibiotic; *Streptococcus*

Introduction

Streptococcus agalactiae (Group B *Streptococcus*: GBS) is the leading cause of bacterial invasive infection during the first 3 months of life (Global Burden of Disease Antimicrobial Resistance Collaborators 2022, Gonçalves et al. 2022). Infection of the newborn mainly occurs vertically during parturition in case of colonization of the mother vaginal tract. Prenatal screening and intrapartum antibiotic prophylaxis (IAP) decrease bacterial burden and risk of invasive infection during the first week of life (Paul et al. 2023). Beta-lactam antibiotics, especially penicillin G and amoxicillin, remain the first-line antibiotics for IAP and early neonatal infections. Despite decades of selective pressure, no ß-lactam resistant GBS isolates have been identified to date. Similarly, the closely related opportunistic pathogen *Streptococcus pyogenes* (Group A *Streptococcus*: GAS) remains sensitive to ß-lactams despite their widespread use to treat common respiratory tract infections. The scientific and clinical communities have long been puzzled by this fortunate situation (Horn et al. 1998). However, the recent isolation of non-susceptible clinical isolates suggests that the situation is evolving (Seki et al. 2015, Metcalf et al. 2017). The nonsusceptible isolates have increased minimal inhibitory concentrations (MICs), which remains below or close to the clinical susceptibility breakpoint. The reduced susceptibility is due to mutations in the *pbp2x* gene encoding the main target to which penicillin G binds (Kimura et al. 2015, Chochua et al. 2022). Mutations in a penicillin-binding protein (PBP) are often a first step toward resistance, which requires additional mutations to compensate for their fitness cost. For instance, isolation of nonsusceptible *Streptococcus pneumoniae* isolates was rapidly followed by the emergence of ß-lactam resistance, a process facilitated by the pneumococcal competence machinery (Albarracin Orio et al. 2011, Gibson et al. 2022, Nishimoto et al. 2022).

In addition to PBP mutations and acquisition of nonsusceptible PBP variants or ß-lactamases, additional mechanisms contribute to ß-lactam resistance in pathogenic species. Especially, mutations in the GdpP phosphodiesterase have been recently described

Received 6 May 2024; **revised** 3 June 2024; **accepted** 11 June 2024

in *S. pneumoniae* and *mec*-negative *Staphylococcus aureus* clinical isolates with low-level ß-lactam resistance (Argudin et al. 2018, Ba et al. 2019, Giulieri et al. 2020, Sommer et al. 2021, Kobras et al. 2023). The GdpP enzyme hydrolyzes cyclic-di-AMP (cdA), a signaling nucleotide acting as second messenger essential for growth under standard conditions. The synthesis of cdA is closely linked to the synthesis of the cell wall, which is essential for resisting turgor pressure and maintaining cell integrity (Corrigan et al. 2011, Massa et al. 2020). The essential enzyme GlmM, which synthesizes an early cell wall metabolite, interacts with and inhibits the cdA cyclase DacA, while the corresponding genes are cotranscribed from a conserved operon (Zhu et al. 2016, Tosi et al. 2019, Gibhardt et al. 2020). However, cdA itself does not appear to directly regulate cell wall synthesis. The cdA mode-of-action primarily depends on regulating transporters involved in the import of potassium and zwitterionic osmolytes (e.g. trimethylglycine also called betaine) necessary to maintain osmotic homeostasis (Stülke and Krüger 2020). In addition to directly modulating transporter activities, cdA also regulates their expression by species-specific mechanisms involving either two-component systems (Moscoso et al. 2015, Gibhardt et al. 2019), transcriptional regulators (Devaux et al. 2018, Pham et al. 2018, Oberkampf et al. 2022), or riboswitches (Nelson et al. 2013, Gundlach et al. 2017). Osmotic homeostasis is primarily achieved by osmolytes transporters but is also coupled to metabolic and physiological responses (Rojas and Huang 2017). In some species, cdA signaling evolves to regulate the tricarboxylic acid cycle (Sureka et al. 2014, Choi et al. 2017) and the general stress response mediated by the Rel enzyme synthesizing the alarmone (p)ppGppp (Peterson et al. 2020, Krüger et al. 2021, 2022, Covaleda-Cortes et al. 2023).

Mutations in cdA metabolic enzymes have been associated with ß-lactam susceptibility or resistance in several species, including laboratory and clinical isolates, but the underlying mechanism remains unclear (Luo and Helmann 2012, Rismondo et al. 2015, Whiteley et al. 2017, Pham et al. 2021, Nolan et al. 2022, Oberkampf et al. 2022). In this study, we first investigated whether cdA has a conserved role in susceptibility to ß-lactams in the almost universally susceptible GBS pathogen. Then, we characterized the cdA signaling pathway and show that osmolyte transporters individually contribute to ß-lactam susceptibility and that their coregulation by cdA, directly and at the transcriptional level via the BusR regulator, confers ß-lactam tolerance. A genome-wide screen of ß-lactam decreased susceptibility confirms the role of cdA signaling and identifies additional pathways, including a conserved RNA-binding protein with a predicted Hfq-like sRNA chaperone activity. This study reveals the molecular basis of cdA-dependent ß-lactam tolerance and prompts an in-depth surveillance and characterization of mechanisms that can promote the development of resistance in pathogens that are still susceptible to this precious class of antibiotic.

Materials and methods

Bacterial strains and culture conditions

The NEM316 (CC-23) and BM110 (CC-17) strains are clinical isolates of capsular serotype III with sequenced genomes available under the NCBI references RefSeq NC_004368 (Glaser et al. 2002) and NZ_LT714196 (Da Cunha et al. 2014), respectively. Strains were grown in Todd-Hewitt supplemented with 1% yeast extract and buffered with 50 mM HEPES pH 7.3 (THY) incubated at 37°C in static condition. Growth curves were done in 96-well microplates (clear, flat bottom, Thermo Scientific) with 150 µl of diluted overnight culture (1/500) by well. Optical density (OD_{600}) was automatically recorded every 10 min with 1 min agitation by cycle at 37°C (TECAN Infinite). Doubling times are determined by fitting nonlinear regression with a Malthusian growth model (GraphPad Prism 10) in exponential phase ($R^2 > 0.99$). Chemically defined medium is prepared as described (Devaux et al. 2018) from a 2-fold stock solution without glutamine and potassium. Glutamine (2 mM) and indicated concentration of potassium and betaine are added extemporaneously, altogether with 2-fold melted BactoAgar solution.

Escherichia coli strains (TOP10, Invitrogen or XL1-blue, Stratagene) used for vector construction were grown in LB with appropriate concentrations of antibiotics (ampicillin 100 µg/ml, kanamycin 25 µg/ml, or erythromycin 150 µg/ml). For selection and propagation of vector in GBS, THY is supplemented with erythromycin (10 µg/ml) or kanamycin (500 µg/ml).

Antibiotic susceptibility tests

MIC in liquid is done following EUCAST guidelines in Mueller–Hinton Fastidious culture media (MH-F, Becton Dickinson) media using custom AST Sensititre 96-well plates (ThermoScientific) and 18 h of incubation at 37°C. Minimal Bactericidal Concentration (MBC) is done by numerating the number of viable bacteria by colony-forming units after MIC determination. MIC on agar plates is done with Etest strips (BioMerieux) on MH-F agar uniformly inoculated with a standardized bacterial solution (5×10^8 CFU/ml) according to EUCAST guidelines.

Spotting assays are done on THY agar supplemented with the indicated concentration of antibiotic. Stocks solution of Penicillin G (1 mg/ml) are aliquots and stored at −20°C for single used and THY plates containing penicillin are prepared and used the same day. Overnight cultures are serial diluted (10-fold factor: 10^{-1} to 10^{-5}) in PBS and 4 µl of each dilution is spotted at the surface of THY plates with and without antibiotic. Incubation is at 37°C in aerobic condition with 5% CO_2.

Time-killing by spotting assay. Cultures in early logarithmic growth phase ($0.3 < OD_{600} < 0.4$) in THY are adjusted to 10^8 CFU/ml and 0.9 ml are distributed in 96 deep-well plates. Sterile water or 10-fold concentrated penicillin are added (0.1 ml), homogenized (MixMate, Eppendorf), and plates are incubated at 37°C. At the indicated time, cultures in deep-well plates are homogenized (MixMate) and an aliquot (50 µl) is taken, serial diluted in PBS (10^{-1} to 10^{-5}) in a 96-well plate and spotted on THY without antibiotic. All steps are done with multichannel pipettes to uniformize time of antibiotic exposure between samples.

Time-killing by CFU quantification. Penicillin was added (time O) in 10 ml of adjusted cultures (10^8 CFU/ml) in early logarithmic growth phase in THY. Incubation was resumed at 37°C and aliquots were taken at the indicated times. Serial dilutions in PBS (10-fold factor) were spread on THY without antibiotic to quantify the number of viable bacteria at each time points. Survival is the ratio of CFU at time X against CFU at time O.

TD-Test for antibiotic tolerance. The original TD-test (Gefen et al. 2017) was adapted for GBS as described for *S. aureus* (Kotkova et al. 2019). First, a disk-diffusion assay was performed on MH medium uniformly inoculated with diluted GBS cultures and with penicillin disks (0.1–10 µg). After overnight incubation at 37°C in 5% CO_2 atmosphere, penicillin disks are removed and carefully replaced by sterile disks containing glucose (10 µg). Tolerance is manifested by bacterial regrown into the initial inhibition zones after an additional incubation at 37°C in 5% CO_2 atmosphere for 24 h.

Bacterial genetic and genome sequencing

All the mutants used in this study, together with the summary of genome sequencing, are described in Supplementary Table S2. Oligonucleotides and construction of vectors are detailed in Supplementary Table S4. Deletion vectors were constructed by splicing-by-overlap PCR using high-fidelity polymerase (Thermo Scientific Phusion Plus) and Gibson assembly into the pG1 thermosensitive shuttle vector as described (Devaux et al. 2018). Final PCR products contain the desired mutations flanked by 500 bp of sequences homologous to the target loci and end with 25 bp of sequences complementary to the pG1 vector. After Gibson assembly, vectors are introduced in *E. coli* XL1 blue (Stratagene) with erythromycin selection. Vector inserts are validated by Sanger sequencing (Eurofins Genomics).

Vectors are introduced in GBS by electroporation. Transformants are selected at 30°C (pG1 permissive replication temperature) with erythromycin. Integration of the vector by homologous recombination at the targeted loci is selected by streaking transformants on THY supplemented with erythromycin and incubated at 37°C (nonpermissive temperature) and further isolation of single colonies in the same condition. Loss of the chromosomally integrated vector occurs through subcultures ($n = 3–5$) in THY at 30°C without antibiotic selective pressure. Single colonies were tested ($n = 24–48$) for the loss of the vector (erythromycin susceptibility) and by discriminatory PCR (MyTaq HS—Bioline) with specific oligonucleotides to select mutant over wild-type (WT) genotypes.

Genomic DNA were purified following manufacturer instruction for Gram-positive bacteria (DNeasy Blood and Tissue—Qiagen) and sequenced (Illumina sequencing at Core facility or Eurofins Genomics). High quality reads in FASTQ were mapped against the reference genome (162-fold coverage mean) and analysed with Geneious Prime (2019.2.3–Biomatters Ltd).

c-di-AMP quantification

Cyclic-di-AMP concentration was determined by LC-MS/MS following company's instruction (Biolog LSI) and as previously described for GBS (Devaux et al. 2018). Bacterial cultures in exponential growth phase were pelleted, washed with PBS, resuspended in 300 µl of nucleotide extraction buffer (acetonitrile/methanol/water; 2/2/1), incubated 15 min on ice, heated 10 min at 95°C, and incubated for an additional 15 min on ice. Cells were lysed by mechanical sharing with 0.1 µM beads (Precellys Evolution, Bertin) and clear lysates were recovered after centrifugation at 4°C. Lysis was repeated two times on cell debris with 200 µl of extraction buffer each time. Clear lysates were pooled and incubated 16 h at −20°C for protein precipitation. After centrifugation (20 min, 4°C), supernatants were recovered and the whole extract was evaporated to dryness (Eppendorf Concentrator). Dry samples were sent to Biolog LSI for nucleotide quantification by LC-MS/MS. For sample normalization, total protein concentration was determined in the initial bacterial cultures.

Electronic microscopy

Bacteria were grown in THY at 37°C until early logarithmic growth phase, harvested by centrifugation, washed twice in PBS, and fixed by incubation in a solution of 4% paraformaldehyde and 1% glutaraldehyde in 0.1 M phosphate buffer (pH 7.2) for 24 h. After two-step washing in PBS, bacteria were postfixed in 2% osmium tetroxide for 1 h and dehydrated in graded ethanol solutions. For scanning electron microscopy (SEM), samples were finally dried with hexamethyldisilazane, coated with platinum by sputtering, and observed with a Zeiss Ultra Plus SEM (Microscopy Department, University of Tours). For transmission electron microscopy (TEM), samples were embedded in Epon resin and allowed to polymerize for 48 h at 60°C. Ultrathin sections of 90 nm were obtained, deposited on EM gold grids, and stained with 5% uranyl acetate and 5% lead citrate, before observation using a JEOL JEM-1011 microscope (Microscopy Department, University of Tours).

RNA sequencing and analysis

RNA purification, sequencing, and analysis were done as described (Mazzuoli et al. 2021). Total RNA was purified from three independent cultures done on different days. The culture conditions are THY inoculated (1/50) with an overnight culture and incubated at 37°C in static condition until exponential growth phase ($OD_{600} = 0.5$). Bacteria are harvested by centrifugation (5 min, 4°C) and washed with 1 ml cold PBS containing RNA stabilization reagents (RNAprotect, Qiagen) before flash freezing and storage at −80°C. Total RNA are extracted after cell wall mechanical lysis with 0.1 µm beads (Precellys Evolution, Bertin Technologies) in RNApro reagent (MP Biomedicals), and purified by chloroform extraction and ethanol precipitation. After resuspension in water (Invitrogen), residual DNA is removed (TURBO DNase, Ambion), RNA concentrations are quantified with fluorescent dye (Qubit RNA HS, Invitrogen) and RNA qualities are validated by electrophoresis (Agilent Bioanalyzer 2100).

Depletion of rRNA (FastSelect Bacterial, Qiagen), libraries construction (TruSeq Stranded mRNA, illumine), and sequencing (NextSeq 500, Illumina) were done following the manufacturers' instructions. Single-end strand-specific 75 bp reads were cleaned (cutadapt v2.10) and mapped on the GBS genomes (Bowtie v2.5.1). Gene counts and differential expression were analysed using DESeq2 (v1.30.1) in R (v4.0.5) (Love et al. 2014). Normalization, dispersion, and statistical tests for differential expression were performed with independent filtering. Raw *P*-values were adjusted for each comparison (Benjamini and Hochberg multiple tests) and adjusted *P*-value lower than .05 were considered significant.

Transposon mutagenesis

A minimal mariner transposon was constructed by PCR with oligonucleotides containing the inverted repeat, modified to contain MmeI restriction sites, used to amplify the kanamycin resistant marker of the pTCV vector (Supplementary Table S4). The purified and digested PCR product was cloned between the EcoRI–BamHI restriction sites of the thermosensitive pG1 vector. A second PCR was done to amplify the Himar9 hyperactive transposase encoding gene under the control of a *gyrA* constitutive promoter. The PCR product was cloned between BamHI–PstI restriction sites to give the pG_TnK vector.

The pG_TnK vector is introduced in GBS by electroporation with erythromycin selection at 30°C (permissive temperature of replication for the vector). Transformants are isolated and cultured in the same condition. After an overnight culture, a starting culture is inoculated (1/25) in THY without antibiotic and incubated at 37°C (nonpermissive temperature of replication for the vector) for 2–4 h. Dilutions (5–10-fold) were spread on THY with kanamycin (500 µg/ml) and incubated at 37°C. To control for vector loss and estimate transposition frequency, dilutions were also spread on THY at 30°C and 37°C (total CFU), and THY with erythromycin at 30°C (total CFU containing the vector) and 37°C (chromosomal integration or mutation of the vector). From four biological replicate, transposition frequency is between 1.5×10^{-4} and 5.9×10^{-5} with 88.1%–94.4% of kanamycin resistant—erythromycin

susceptible colonies corresponding to chromosomally integrated TnK and loss of the vector backbone.

A total of 176 THY kanamycin plates inoculated from four independent starting cultures and with 5×10^2–10^3 colonies after incubation at 37°C were used to constitute the library collection. Bacteria were gently recovered with 4 ml of THY by plate, pooled, centrifuged (10 min, 4°C), washed with THY, resuspend in 4 × 25 ml glycerol 20%, and stored at −80°C by aliquots of 1.5 ml. Single tube were used for numeration on THY kanamycin at 37°c and single colonies were picked to confirmed erythromycin susceptibility ($n = 96$; > 95% ery^S). Genomic DNA of isolated colony were purified from 7.5 ml of culture (DNeasy Blood and Tissue—Qiagen) with an additional step of cell lysis with microbeads (Precellys Evolution). Genomic DNA are used as template for Sanger sequencing with a transposon specific primer (BAC protocol, Eurofins). Sequence reads were mapped against the transposon end and flanking sequences are then mapped against the GBS genome to identify the transposition integration site. For screening, THY were inoculated (1/100) with −80°C library stocks and incubated 1 h at 37°C for recovery before spreading dilutions on freshly prepared THY plates containing increasing concentration of penicillin. Plates are incubated at 37°C in a 5% CO_2 incubator and colonies were further isolated on THY before genomic DNA purification and sequencing of transposon–chromosome junction (Eurofins).

Results

Inactivation of the c-di-AMP phosphodiesterase GdpP confers ß-lactam tolerance

We first investigated whether the second messenger cdA had a conserved role in ß-lactam susceptibility in a species, which has always remained clinically susceptible. In GBS, cdA is synthesized from two ATP molecules by the cyclase DacA and hydrolyzed into pApA by the phosphodiesterase GdpP (Devaux et al. 2018). DacA, and thus cdA synthesis, is essential for growth unless the concentration of osmolytes is tightly limited in the growth medium or compensatory mutations allow growth in usual media. (Devaux et al. 2018). To test the susceptibility to ß-lactams, we therefore used a Δ*gdpP* mutant with a high cdA intracellular concentration made in the NEM316 WT strain (Devaux et al. 2018). First, conventional antibiotics susceptibility testing shows similar MICs for the Δ*gdpP* mutant and the WT control, whether by broth microdilution or by gradient tests using Etests (Fig. 1A).

In contrast, spotting assays reveal growth of the Δ*gdpP* mutant on THY plates containing concentrations of penicillin G and cephalexin that inhibit the WT strain (Fig. 1B). Time-killing experiments with high penicillin concentrations (MIC × 2 < 0.1–10 µg/ml < MIC × 200) added to exponentially growing cultures before spotting on THY plates without antibiotic show that the Δ*gdpP* mutant is killed more slowly than the WT strain (Fig. 1C). Noteworthy, the bactericidal activity is initially inversely proportional to the drug concentration when exceeding four times the MIC, a phenomenon known as the "Eagle effect" and first described in the 1940s for GBS (Eagle and Musselman 1948), for the WT control only (Fig. 1C). Time-killing experiments using CFU counts confirmed the advantage of the Δ*gdpP* mutant, which exhibited a decreased killing rate compared to the WT strain (Fig. 1D). Slow-killing kinetics and no difference between the Δ*gdpP* mutant and the WT strain were observed when stationary phase cultures were used (Fig. 1D), in agreement with the mode of action of ß-lactams requiring active cell wall metabolism and division. Adaptation of the TD-test, a modified disk-diffusion assay for antibiotic tolerance (Gefen et al. 2017, Kotkova et al. 2019), further shows that the Δ*gdpP* mutant can survive lethal concentration of penicillin (Fig. 1E).

To determine whether tolerance is a result of GdpP enzymatic activity, we substituted the conserved catalytic residue D_{419} (Rao et al. 2010, Corrigan et al. 2011) with an alanine by targeted mutagenesis in the WT strain. The $GdpP_{D419A}$ catalytic-minus and the Δ*gdpP* mutants have similar high intracellular cdA concentration and ß-lactam phenotype (Fig. 1F). In addition, complementation of the Δ*gdpP* mutant with a vector containing a WT copy of *gdpP* (pTCV_*gdpP*) abolishes the phenotype of the Δ*gdpP* mutant on penicillin-containing plates (Fig. 1G). Overall, a high intracellular concentration of cdA confers ß-lactam tolerance, characterized by similar MICs but slow-killing kinetics (Brauner et al. 2016), demonstrating that cdA is involved in the response of GBS to ß-lactams.

cdA catabolism impacts physiology, cell envelope, and division

Antibiotic tolerance is frequently dependent on the growth rate and/or metabolic activity of the target cell, especially for ß-lactams (Tuomanen et al. 1986, Lee et al. 2018, Lopatkin et al. 2019). At first glance, the individual growth curves in rich medium (THY) show a fitness defect in the exponential phase for the Δ*gdpP* mutant compared with the WT strain, with a doubling time of 34.4 +/− 0.5 min and 27.2 +/− 1.1 min, respectively (Fig. 2A). However, preliminary microscopic observations revealed significant heterogeneity and major morphological defects in the Δ*gdpP* mutant. Closer examination by SEM and TEM show morphological defects affecting the ultrastructures of the cell surface, both membranous and parietal (Fig. 2B). Instead of chains of dividing cocci, Δ*gdpP* cells are heterogenous, often swollen, with rough surface, and septation defects. Cell envelopes are irregularly thickened, cells are frequently compartmentalized by multiple curved septum-like structures, and invaginated membranous structures are also observed (Fig. 2B and C). The WT morphology is restored in the Δ*gdpP* mutant with the complementing *gdpP* vector but not with the empty vector (Fig. 2D). Overall, the absence of *gdpP* leads to severe morphological alterations, with large effects on cell envelope and division.

The BusR transcriptional repressor antagonizes ß-lactam tolerance

The morphology of the Δ*gdpP* cells suggests large-scale perturbations involving, either directly or indirectly, cell wall synthesis. To characterize the associated stress responses, we analyzed the transcriptome of the Δ*gdpP* mutant in exponential growth phase at 37°C in rich media. In total, 69 genes are significantly differentially expressed (DEG : $|\log_2 FC| > 1$ and $P\text{-adj} < 10^{-4}$), among which 28 are part of multicopy integrative genomic elements known as TnGBS (Guerillot et al. 2013) that we have excluded for the rest of the analysis (Fig. 3A and Supplementary Table S1A). Of the remaining DEG, 11 and 30 are up- and downregulated, respectively. Except for two uncharacterized genes, fold changes and significance are relatively minor (Fig. 3A), and analysis of gene function does not provide a clear pattern (Supplementary Table S1A). To gain confidence, we analyzed the transcriptome of a second Δ*gdpP* mutant made in a different WT background (strain BM110, of the same capsular serotype III and belonging to the hypervirulent clonal complex CC-17; Da Cunha et al. 2014). Applying the same thresholds, 67 DEG were identified including 39 in prophages (Fig. 3A and Supplementary Table S1B). Comparative analysis

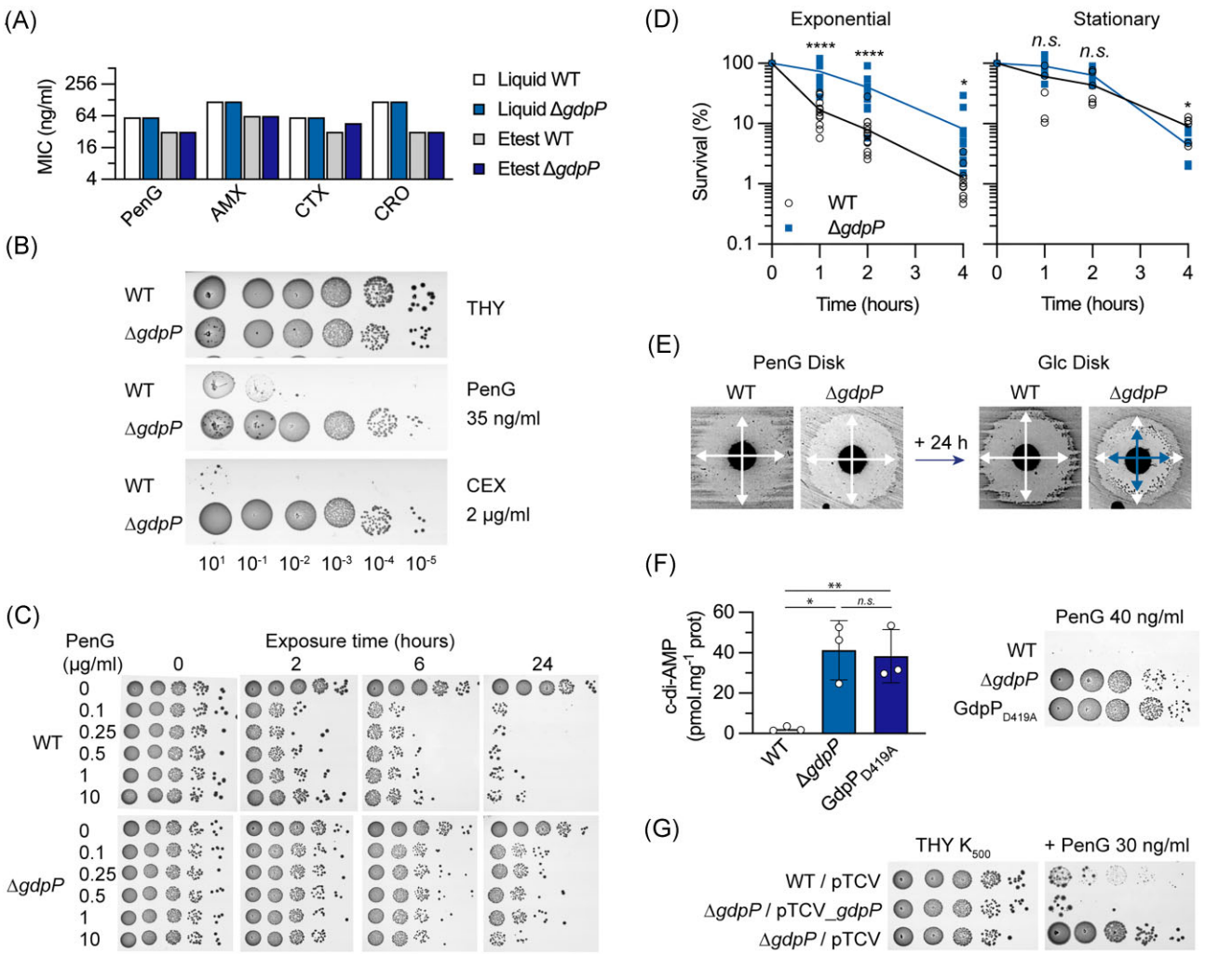

Figure 1. Inactivation of the cyclic-di-AMP phosphodiesterase GdpP confers beta-lactam tolerance. (A) MIC of antibiotics: conventional tests in liquid (broth microdilution) and solid (gradient Etest strips) in MH-F media with the WT strain and the Δ*gdpP* c-di-AMP phosphodiesterase deletion mutant for penicillin G (PenG), amoxicillin (AMX), and the third-generation cephalosporin cefotaxime (CTX), and ceftriaxone (CRO). (B) Spotting assays of the WT strain and Δ*gdpP* mutant: overnight cultures were serially diluted (10^{1}–10^{-5}) and spotted on the surface of THY agar supplemented with PenG or the first-generation cephalosporin cephalexin (CEX). Images were taken after 16–24 h incubation at 37°C in aerobic condition with 5% CO_2. (C) Dose and time-dependent killing of the WT strain and Δ*gdpP* mutant. High PenG concentrations (0.1–10 µg/ml) are added to exponential growing cultures of the WT strain and Δ*gdpP* mutant. Aliquots were taken at the indicate time, serial diluted, and spotted on THY without antibiotic. (D) Time-killing of exponential and stationary phase cultures of the WT strain and Δ*gdpP* mutant in presence of 10 µg/ml PenG. Aliquots were taken at the indicate time and dilution were plated on THY for colony-forming unit numeration. Data are from seven and six independent experiments for exponential and stationary time, respectively. Unpaired *t*-test were used to compare the WT and the mutant at each time point (* $P < .05$; **** $P < .0001$). (E) Adaptation of the TD-test for GBS antibiotic tolerance. Diluted cultures of the WT strain and Δ*gdpP* mutant are spread on MH media and PenG disks (10 µg) were added. After a 24-h incubation, PenG disks were removed and replaced by glucose (Glc) disks (10 mg). Crossed white arrows highlight inhibition zones after 24 h, and crossed blue arrows highlight the decrease in the inhibition zone of the Δ*gdpP* mutant after an additional 24 h incubation with the Glc disk. (F) Penicillin tolerance depends on the GdpP phosphodiesterase activity. Left panel: quantification of intracellular c-di-AMP by LC-MS in the WT strain, the Δ*gdpP* mutant, and the catalytic inactivated $GdpP_{D419A}$ mutant. Data represent means and SD calculated from biological triplicate ($N = 3$) and analyzed with unpaired *t*-test (* $P < .05$; ** $P < .01$). Right panel: spotting assays on PenG plate. (G) Genetic complementation of the Δ*gdpP* mutant. Spotting assay with the WT and the Δ*gdpP* mutant containing the empty (pTCV) or complementing (pTCV_*gdpP*) vectors. Kanamycin (K_{500}) is added to maintain the selective pressure for the vectors.

between the two backgrounds reveals only 22 genes with a conserved significant differential expression (P-adj < 10^{-4}), among which only 10 with a conserved threshold above $|\log_2 FC| > 1$ (Fig. 3B and Supplementary Table S1C and S1D). Overall, transcriptomes suggest a strain-specific adaptation to the absence of *gdpP*, but do not allow to unambiguously identify a conserved response.

Despite the relatively low level of information provided by RNA-seq analysis, we and others have previously shown that the BusR transcriptional regulator is allosterically activated by cdA and directly represses the *busAB* operon encoding a betaine transporter (Devaux et al. 2018, Pham et al. 2018, Bandera et al. 2021, Oberkampf et al. 2022). Consistently, *busAB* genes are among the most repressed in the Δ*gdpP* mutants but reach statistical significance in the NEM316 background only (Fig. 3B). This indicates that the BusR repressor is active in the WT strains and overactivated by the high cdA concentration in the Δ*gdpP* mutants. We, therefore deleted *busR* in the WT strains and in their corresponding Δ*gdpP* mutants to test ß-lactam susceptibilities. Deletion of *busR* is associated with a fitness cost, especially in the Δ*gdpP* backgrounds (Supplementary Fig. S1), indicating that BusR must be tightly

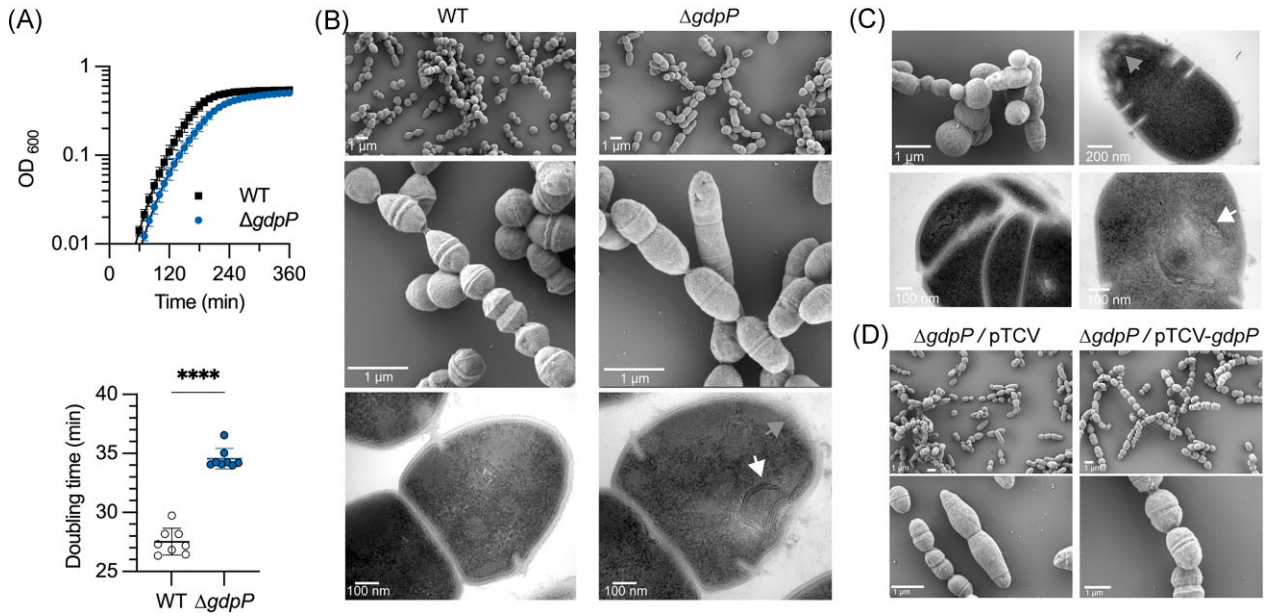

Figure 2. Cyclic-di-AMP phosphodiesterase deficiency leads to morphological and cell envelope defects. (A) Growth curves (upper panel) and doubling time in exponential phase (bottom panel) of the WT strain and Δ*gdpP* mutant in THY at 37°C. Means and SD are calculated from biological replicates ($N = 8$) and analyzed using unpaired *t*-test (**** $P < .0001$). (B) SEM and TEM of the WT strain and Δ*gdpP* mutant at similar scales. The white and grey arrows highlight intracytoplasmic membrane structures and areas with cell envelopes of heterogeneous thickness, respectively. (C) Additional electronic microscopy illustrating the heterogeneity and atypical ultrastructure of Δ*gdpP* cells. (D) Representative images of the Δ*gdpP* mutant with the empty (pTCV) or complementing (pTCV_*gdpP*) vectors observed by SEM.

regulated and that its inactivation is antagonistic with a high cdA concentration. Interestingly, Δ*busR* mutants are more susceptible to penicillin compared to their WT parental strains (Fig. 3C). Moreover, deletion of *busR* in the Δ*gdpP* mutants decreases the growth advantage of the parental Δ*gdpP* mutants on penicillin-containing plates (Fig. 3C). The Δ*gdpP* phenotype is, thus dependent on the transcriptional repressor BusR, which is already active in the WT strain and negatively regulates genes conferring ß-lactam susceptibility.

The BusR signaling pathway regulates ß-lactam susceptibility

To characterize the BusR regulon, we analyzed the transcriptome of the Δ*busR* mutants in the two WT backgrounds (Fig. 3A and B). In addition to *busAB* (FC = 23–64-fold, $10^{-45} < P\text{-adj} < 10^{-140}$), BusR negatively regulates a seven-genes operon thereafter called the *amaP*-operon (FC = 10–37-fold, $10^{-35} < P\text{-adj} < 10^{-78}$) adjacent to, and translated in the same direction as, the *busR* operon (Supplementary Fig. S1 and Supplementary Table S1E). The seven small proteins (65–194 amino acids) encoded in the *amaP*-operon are predicted to form a membrane-localized protein complex with redundant functional subunits (3 x Asp23-domain proteins PF04226/PF03780/DUF322 including AmaP, 2 almost identical GlsB-like proteins PF04226, 1 x DUF2773, and 1 x CsbD-like family PF05532). In addition, one monocistronic gene (*pepY2*, FC = 13–16-fold, $10^{-52} < P\text{-adj} < 10^{-98}$) encoding a predicted transmembrane protein containing two PepSY ectodomains (PF03413) is also highly significantly repressed by BusR (Fig. 3B and Supplementary Table S1E).

The three genetic units (*busAB*, *amaP*-operon, and *pepY2*) define the BusR regulon, which is distinct from the indirect transcriptional perturbations observed in individual Δ*busR* transcriptomes (Fig. 3B). Putative BusR binding sites are detected close to *amaP*-operon and *pepY2* transcriptional start sites suggesting direct BusR-repression (Supplementary Fig. S1), as previously demonstrated for BusR on the *busAB* promoter (Bandera et al. 2021). To test the role of the regulon in the susceptibility of the Δ*busR* mutant to ß-lactams, we deleted *busB*, the whole *amaP*-operon, and *pepY2* in the Δ*busR* mutant (*n.b.* in the NEM316 WT strain only). Deletion of *busB* and of the *amaP*-operon restores the growth of the parental Δ*busR* mutant on penicillin-containing plates (Fig. 3D). Overall, BusR negatively regulates three genetic units, including two that confer susceptibility to ß-lactams susceptibility when BusR is inactive: the betaine transporter BusAB and an AmaP/Asp23/GlsB complex with a probable function in cell envelope homeostasis (Muller et al. 2014, Tödter et al. 2017, Barros et al. 2019). In the context of a Δ*gdpP* mutant with a high level of cdA, BusR is overactivated and the repression of the regulon contributes to the tolerance of the Δ*gdpP* mutant to ß-lactams.

Joint regulation of osmolyte transporter activity and expression confers tolerance to ß-lactams

The opposite but additive ß-lactam phenotypes of Δ*gdpP* and Δ*busR* mutants reveal a mechanism based on cdA activation of the BusR transcriptional repressor. However, the cdA-signaling network in GBS is a set of negative regulations (Fig. 4A), which also includes the direct inhibition of the potassium transporters KtrAB and TrkAH and of the zwitterionic transporter subunit OpuCA (Devaux et al. 2018). In addition, cdA likely inhibits the RCK_C domain containing protein EriC, a chloride channel protein necessary to reestablish the ionic balance after osmolyte uptake (Devaux et al. 2018). Lastly, binding of cdA to the small CBS domain protein CbpB abolishes the CbpB–Rel allosteric interaction leading to decreased (p)ppGpp synthase activity (Covaleda-Cortes et al. 2023), which is a conserved mechanism of antibiotic tolerance (Corrigan et al. 2016, Salzer and Wolz 2023).

All the components of the signaling pathway are inhibited by the high cdA concentration in the Δ*gdpP* mutant. To test

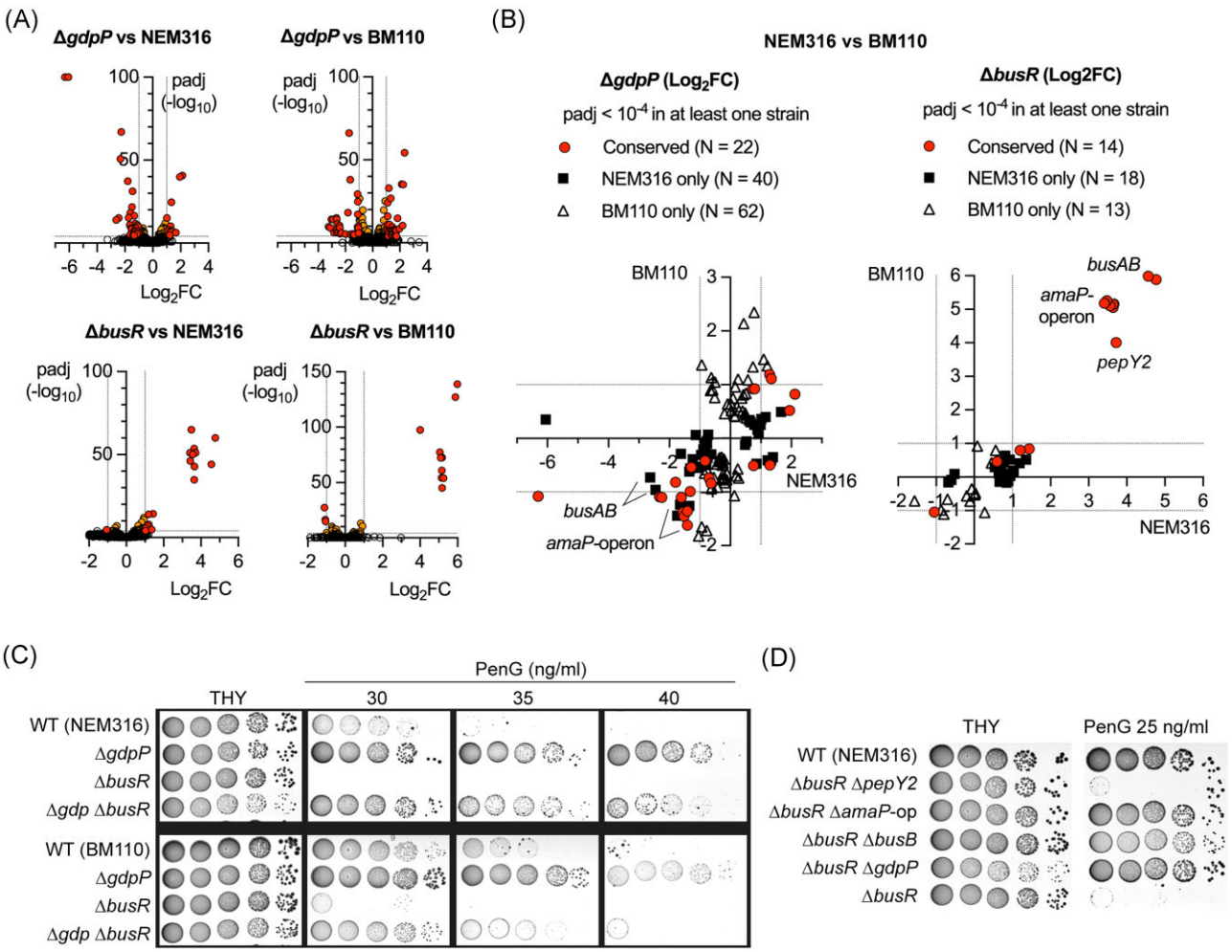

Figure 3. ß-lactam tolerance depends on the c-di-AMP-activated BusR repressor. (A) Transcriptome analysis by RNA-seq of Δ*gdpP* and Δ*busR* mutants in two WT backgrounds (NEM316 and BM110). Colored dots on volcano plots highlight significant differential expression (*P*-adj < 10^{-4}) with fold changes |FC| > 2 (red dots) and |FC| < 2 (orange dots). (B) Comparative analysis of the Δ*gdpP* and Δ*busR* transcriptomes between the two WT backgrounds. Red dots highlight conserved statistical significance (*P*-adj < 10^{-4}) in the two strains, and black squares and white triangles highlight statistical significance in NEM316 only or BM110 only, respectively. (C) Tolerance of Δ*gdpP* to ß-lactam depends on the cdA-activated BusR repressor. Spotting assays (10^{-1}–10^{-5} serial dilution) of Δ*gdpP*, Δ*busR*, and the double Δ*gdpP* Δ*busR* mutants in the two WT backgrounds on THY supplemented with penicillin. (D) Susceptibility of Δ*busR* to ß-lactam depends on *busB* and *amaP* operon. Spotting assays with Δ*busR*, and the double Δ*busR* Δ*pepY2*, Δ*busR* Δ*amaP*-operon, Δ*busR* Δ*busB*, and Δ*busR* Δ*gdpP* mutants in the NEM316 background.

their individual contribution, we used a collection of deletion and insertional mutants in the WT strain (n.b. NEM316). On penicillin-containing plates, the Δ*busA*, Δ*opuCA*:: *TnE*, and Δ*trkA* mutants grow on ß-lactam concentration higher than those inhibiting the WT strain, without reaching the phenotype of the Δ*gdpP* mutant (Fig. 4B). To test whether transporters have cumulative effects, we generated additional single deletion mutants (Δ*busA*, Δ*opu*-operon) and double deletion mutants for the two zwitterionic transporters (Δ*busA* Δ*opu*-op), two potassium transporters (Δ*ktrA* Δ*trkA*), and a pair of potassium-betaine transporters (Δ*trkA* Δ*busB*).

After sequencing the genome of all mutants (Supplementary Table S2A), we identified two issues. First, we unexpectedly identified two different NEM316 WT profiles, differing by 14 and 8 SNPs (five in common) compared to the reference sequence (Supplementary Table S2B). The 14 SNPs profile was already reported (Mazzuoli et al. 2021) and the eight SNPs profile corresponds to the oldest mutants generated in the laboratory [Δ*gdpP* (Devaux et al. 2018) and Δ*opuCA*:: *TnE* (Firon et al. 2013)]. Although the Δ*gdpP* phenotypes are complemented (Figs 1 and 2) and out of cautious, we constructed a new mutant (Δ*gdpP*-2) in the 14 SNPs profile and validated the absence of any secondary mutation (Supplementary Table S2A). Second, the *pepY2* mutants have secondary mutations in *glsB* or *lysM* genes, which we cannot exclude as compensatory mutations (Supplementary Table S2C). Consequently, the noninvolvement of *pepY2* in ß-lactam susceptibility is not conclusive at this stage.

Focusing on potassium and zwitterionic transporters, parallel phenotypic analysis reveals three degrees of penicillin susceptibility. First, inactivation of the BusAB or OpuCA zwitterionic transporters confers a slight advantage in the presence of penicillin (Fig. 4C). The phenotype is similar between single deletion mutants and is not additive (Fig. 4C). Second, inactivation of the potassium importer TrkA leads to a stronger phenotype closer to Δ*gdpP* mutants. Third, inactivation of either the BusAB or KtrA transporter in the Δ*trkA* mutant further increases the growth advantage of the Δ*trkA* single mutant to a level even slightly superior to the Δ*gdpP* mutant (Fig. 4C). These results show that the Δ*gdpP* ß-lactam tolerance is potentiated by the simultaneous inactivation of potassium and zwitterion importers. Notably, the stronger

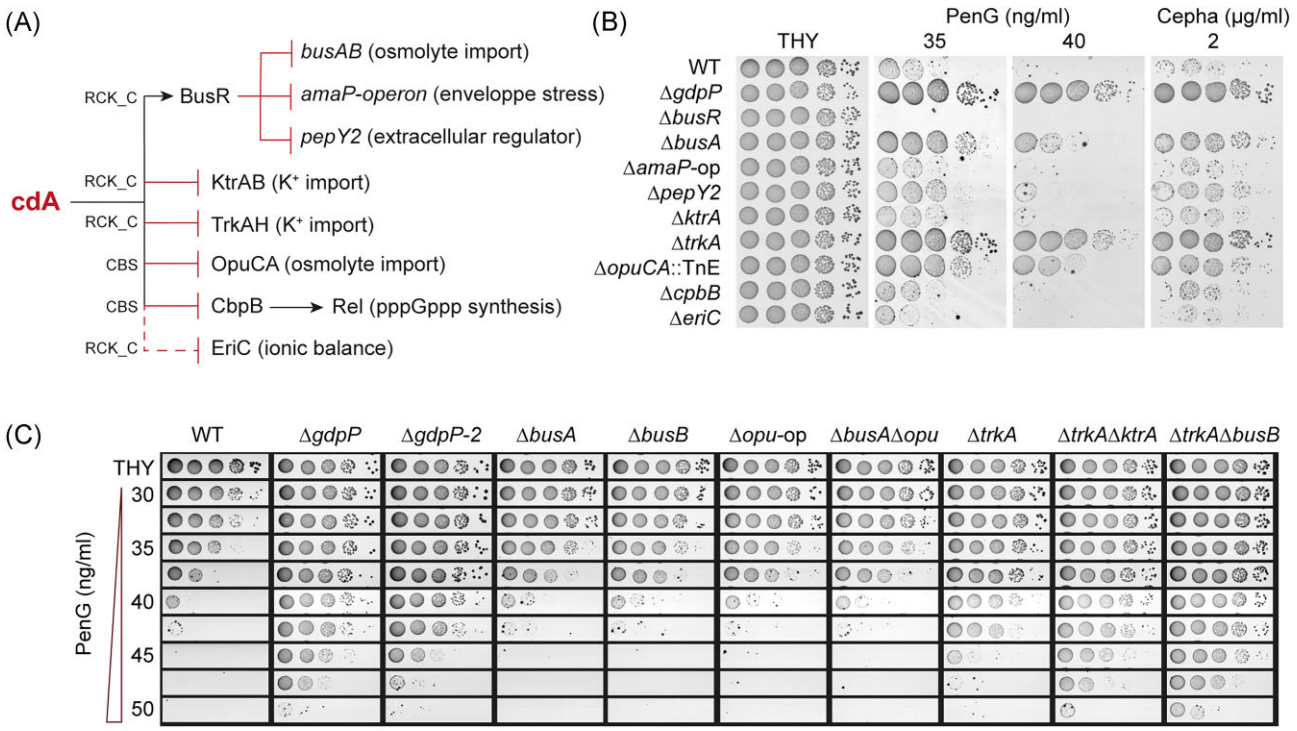

Figure 4. Coordinated regulation of osmolyte transporters confers ß-lactam tolerance. (A) Diagram of the c-di-AMP (cdA)-signaling network in GBS. The cdA-binding domain (RCK_C or CBS) of each effector is indicated on the connecting lines, with arrows indicating activation and final bars indicating repression or inhibition. The dotted line denotes predicted cdA binding to the RCK_C domain of EriC that has not been demonstrated experimentally. (B) Individual effectors contribute to ß-lactam susceptibility. Spotting assays (10^{-1}–10^{-5} serial dilution) of a collection of deletion (Δ) or insertion (:: TnE) mutants for each individual cdA effector on ß-lactam-containing plates. (C) Additive effect of cdA effectors on penicillin susceptibility. Spotting assays of single and double deletion mutants on plates containing increasing concentrations of penicillin, in increments of 2.5 ng/ml. An independent Δ*gdpP*-2 mutant was included for validation.

phenotype is associated with the inhibition of potassium uptake, which is the first cellular response in case of hyperosmotic stress. The contribution of the second cellular response, the uptake of zwitterion to compensate the deleterious effects of potassium, is dependent on the BusR regulator and is dampened by transporters redundancy. Altogether, this reflects the dynamics of osmolyte exchanges coordinated by cdA through direct inhibition (KtrA, TrkA, and OpuCA) and transcriptional repression (*busAB* through BusR activation).

cdA primes cells against penicillin-induced osmotic shock

We next sought to test the effect of potassium and zwitterions on the Δ*gdpP* ß-lactam phenotype. Interestingly, we observed a "mirror" phenotype on synthetic minimal media containing only trace amount of potassium (Fig. 5A). As expected, the WT strain grows on minimal media and is inhibited by the addition of penicillin. At the opposite, the Δ*gdpP* mutant is unable to grow unless penicillin is added (Fig. 5A). The addition of betaine (5 mM) circumvents the need for penicillin and restores Δ*gdpP* growth, while the addition of potassium (0.1, 0.5, or 5 mM) has a marginal effect, and the two osmolytes do not influence the growth of the mutant in the presence of penicillin (Fig. 5A). Altogether, this suggests that the cdA-inhibition of high affinity osmolyte transporters inhibits the growth of the Δ*gdpP* mutant and that penicillin weakens the cell wall allowing osmolyte uptake.

The Δ*gdpP* mutants have been previously demonstrated to be susceptible to hyperosmotic stress in GBS and other species due to the inhibition of osmolyte transporters required to re-establishes the turgor pressure (Muller et al. 2014, Tödter et al. 2017, Barros et al. 2019). To test whether cell wall rigidity contributes to the Δ*gdpP* osmo-susceptibility, we added subinhibitory concentrations of penicillin to high osmolarity growth medium. Strikingly, cell wall fluidization by subinhibitory concentrations restores the growth of the Δ*gdpP* mutant in hyperosmotic condition (Fig. 5B). Overall, this suggests that the Δ*gdpP* mutant is in a physiological state corresponding to hyperosmotic stress under normal growth conditions (Fig. 5C). The Δ*gdpP* mutant is unable to cope with standard hyperosmotic stress, but its reduced turgor pressure confers an advantage when challenged with the bactericidal activity of penicillin (Fig. 5C).

Convergent mutations impact ß-lactam susceptibility

Catabolism of cdA is the first mechanism involved in ß-lactams tolerance reported in GBS. To extend the analysis, we screened a pool of 1.2 × 10^5 random insertional mutants under conditions that allowed growth of the Δ*gdpP* mutant but not the WT strain (Supplementary Fig. S2). Bacterial viability of the insertional mutant collection decreased by a 100-fold factor on plates containing 30 ng/ml penicillin, with further 10-fold reduction in viability per 5 ng/ml drug increment (Supplementary Fig. S2). As control, we first sequenced the transposon-chromosome junction in 240 colonies isolated on THY without antibiotic, confirming that integration of the transposon is randomly distributed along the chromosome (Fig. 6A and Supplementary Table S3A). After selection for ß-lactam tolerance, sequencing of the transposon–chromosome junctions in 191 colonies isolated from

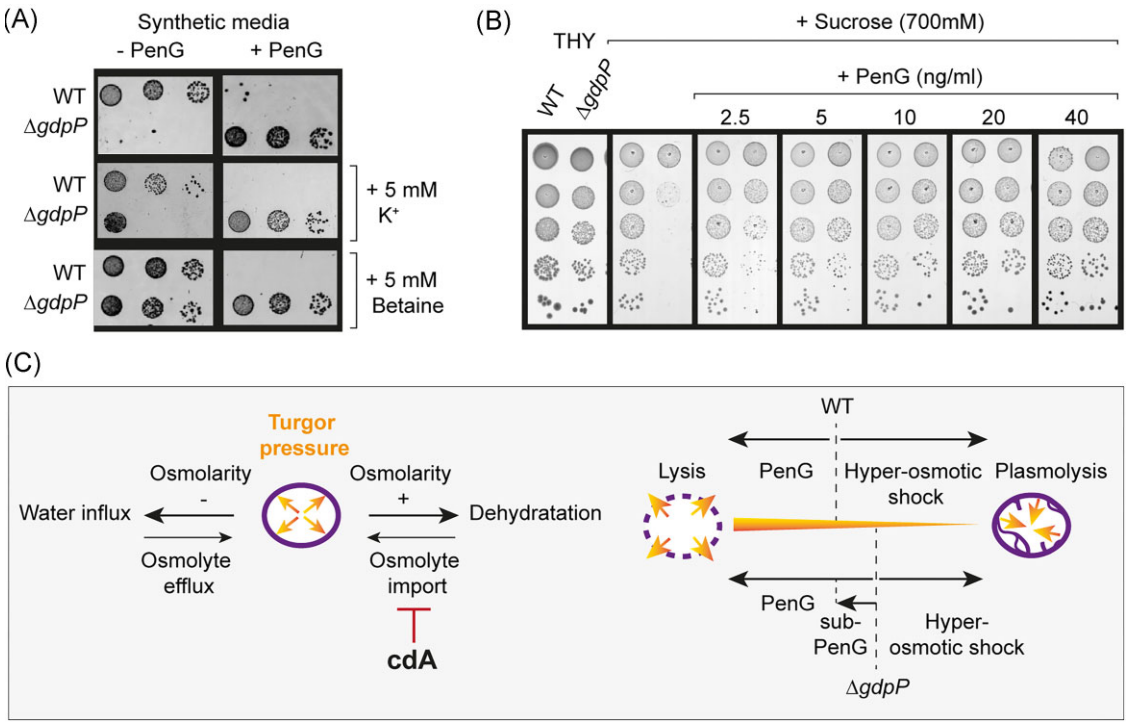

Figure 5. C-di-AMP balances osmotic and ß-lactam susceptibilities. (A) Penicillin alleviates Δ*gdpP* osmolyte requirements on minimal media. Spotting assays of the WT strain and Δ*gdpP* mutant on synthetic media supplemented with penicillin, potassium, and betaine at the indicated concentration. (B) Subinhibitory ß-lactam concentrations counteract Δ*gdpP* osmo-susceptibility. Spotting assays of the WT strain and Δ*gdpP* mutant under hyperosmotic condition (THY supplemented with sucrose) with and without penicillin. (C) Osmotic regulation by cdA and adaptation to osmotic imbalances. Left panel: the cellular turgor pressure is mainly regulated through osmolytes exchanges to respond to change in osmolarity. The import of osmolytes is necessary to counteract cellular dehydration due to increased osmolarity and is inhibited by cdA. Right panel: the high cdA concentration in the Δ*gdpP* mutant results in a hyperosmotic stress physiology in a standard environment. The advantage against the bactericidal activity of ß-lactam is at the cost of sensitivity to hyper osmotic condition. Fluidification of the cell wall with ß-lactam subinhibitory concentration allows osmolyte exchange and re-establishes a WT-like turgor pressure.

the 35 and 40 ng/ml screening plates shows a highly biased insertion of the transposon at specific loci (Fig. 6A), with 69% (132/191) of the insertions into 5 genes at 29 independent chromosomal positions (Supplementary Fig. S2 and Supplementary Table S3).

We selected 16 mutants with insertions in 12 genes, based on the number of independent insertions and on functional annotation. We also added one mutant with an insertion of the transposon into *gdpP*. All isolated transposon mutants grew at concentrations of penicillin that inhibited the WT strain (Fig. 6B) and, as expected, the *gdpP*:: TnK and Δ*gdpP* mutants have a similar phenotype. Remarkably, 12 insertional mutants grow on penicillin-containing plates at concentration that inhibits the *gdpP* mutants (Fig. 6B). All mutants have similar ß-lactams MIC, within a 2-fold factor of the WT MIC (Fig. 6C). The MBC after 16 h of contact with ß-lactams are similar to the MIC for all mutants, giving an MBC/MIC ratio close to 1 (Fig. 6C), far from the threshold defining clinical antibiotic tolerance (MBC/MIC ≥ 32).

Genome sequencing of the 16 selected insertional mutants confirmed the transposon integration sites and reveals a convergent pattern of mutations in four genes: *gh25*, *khpB* (also called *jag*)—*khpA*, and *ess* (Fig. 6B). In addition to the mutation due to transposon integration, each mutant has between two and five secondary mutations (Supplementary Fig. S3 and Supplementary Table S3D). The *gh25* gene is the most frequently inactivated gene in the initial screen (63/191 = 33% of the insertions, at six independent position) and is also inactivated by secondary mutations in 6 of the other 15 mutants selected for individual screening (Fig. 6B and Supplementary Fig. S3). The *gh25* gene encodes for a secreted cell-wall lytic enzyme with a predicted lysozyme activity (GH25, glycosyl hydrolase family 25, PF01183). This enzyme is a candidate for being the main peptidoglycan hydrolase required for the bactericidal activity of ß-lactams in GBS (Cho et al. 2014, Wang et al. 2022a).

Three independent transposon insertions occur in the two subunits of the small RNA chaperone KhpAB, with loss-of-function secondary mutations in *khpB* also present in two additional TnK mutants (Fig. 6B and Supplementary Table S3D). KhpAB homologues have been recently associated with ß-lactam sensitivity and/or cell wall synthesis in several Firmicutes (Zheng et al. 2017, Olejniczak et al. 2022, Michaux et al. 2023), suggesting a conserved cellular function based on small RNA regulation. Independent mutations in the *ess* gene, encoding the protein S initially described as necessary for immune evasion, suggest a cell wall related function depending on the LysM peptidoglycan-binding domain of the protein (Wierzbicki et al. 2019, Campeau et al. 2021). Notably, combination of mutations between *gh25*, *khpAB*, and *ess* are frequently observed (Fig. 6B and Supplementary Fig. S3). This suggests that a first mutation in one of the four genes promotes the selection of mutations in the other genes, leading to additive phenotypes between functionally interacting pathways. Finally, other mutations in a transporter (*bmp2*: stand-alone ABC solute transporter) and metabolic (*codY*) genes also lead to increase tolerance on plates. Overall, the GBS response to ß-lactams involved conserved and specific genes, including a core of four overlooked genes encoding cell-wall related functions.

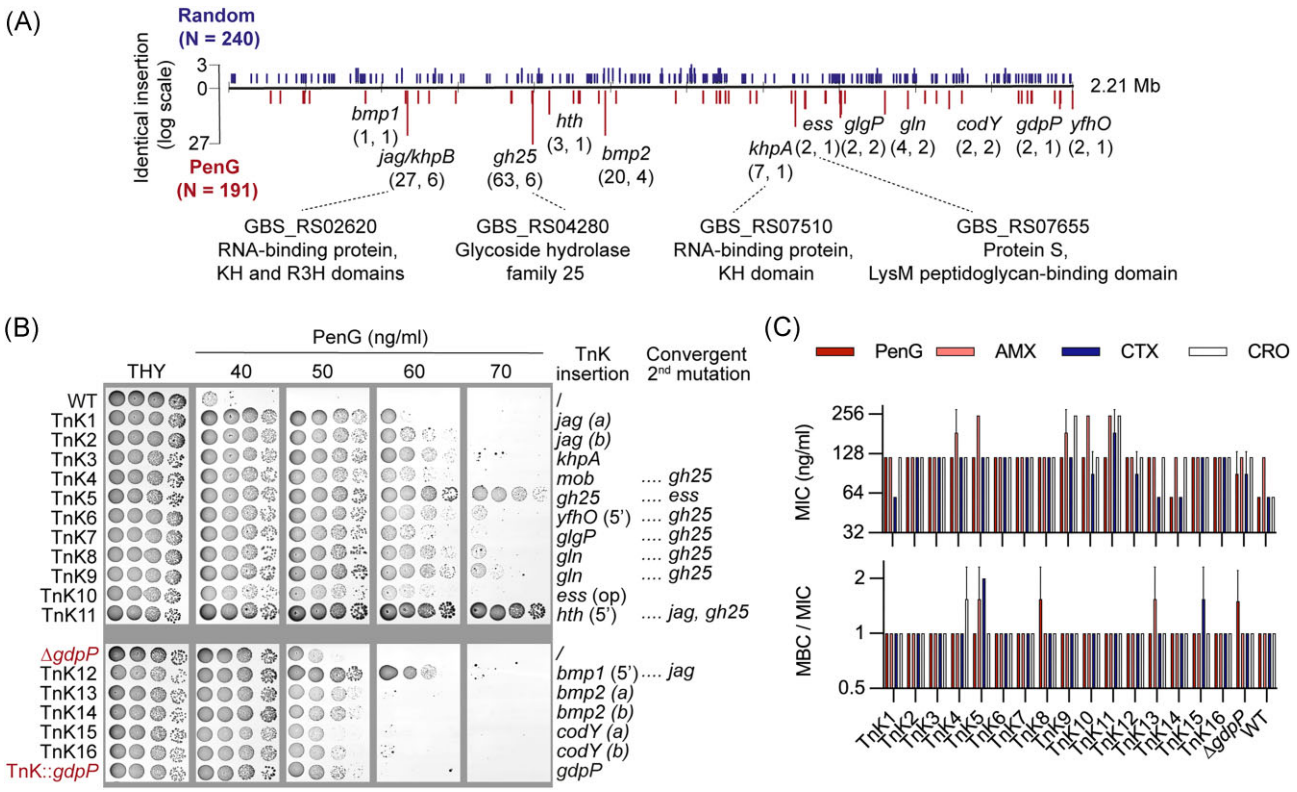

Figure 6. Genome-wide screening for ß-lactam tolerance in GBS. (A) Distribution of transposon insertions on the GBS chromosome. Vertical bars represent identical transposon insertions along the 2.1-Mb genome in randomly isolated colonies on THY ($N = 240$, upper blue bars) or THY supplemented with 35–40 ng/ml PenG ($N = 191$, lower red bars). Gene names are specified for mutants selected for secondary screening. The numbers in brackets indicated the total number of transposon insertions followed by the number of independent integration sites. Gene IDs and predicted functions are shown for the four genes showing a convergent mutation pattern. (B) Spotting assay with isolated insertional mutants (TnK) on plates with increasing PenG concentration. Genes inactivated by transposon insertion are indicated on the right, with independent insertion in the same gene indicated by letters (a and b), and whether the insertion is in the promoter (5') or in nonmonocistronic transcripts (-op). Convergent secondary mutations identified after genome sequencing are indicated after the dotted lines. Deletion (Δ) and insertional (Tnk::) *gdpP* mutants are highlighted in red. (C) MIC and MBC for ß-lactams. MIC are determined in liquid (MH-F media) by serial dilution for penicillin G (PenG) amoxicillin (AMX), cefotaxime (CTX), and ceftriaxone (CRO). MBC are determined by numeration of viable bacteria after 16 h of contact with the antibiotic in MH-F. Data are mean and SD of two independent experiments ($N = 2$).

Discussion

The cyclic-di-AMP signaling nucleotide is an essential regulator of bacterial physiology (Stülke and Krüger 2020) and has emerged as a key determinant of low-level ß-lactam resistance in pathogenic species (Argudin et al. 2018, Ba et al. 2019, Giulieri et al. 2020, Sommer et al. 2021, Kobras et al. 2023). This study shows that cdA is a conserved regulator of ß-lactam antibiotic response in a historically clinically sensitive species. Mechanistic analysis of the cdA signaling network reveals an integrated pathway dedicated to the maintenance of osmotic homeostasis in which individual effectors contributes to the overall response. Our model can be applied generically but needs to consider the unique characteristics of each species.

Our results provide evidence that regulation of cell turgor is the main mechanism underlying cdA-related cell wall phenotypes (Commichau et al. 2017, Commichau and Stülke 2018). Inactivation of GdpP leads to resistance or tolerance to ß-lactam antibiotics and, at the opposite, absence of cdA synthesis is associated with increased susceptibility (Commichau et al. 2017, Commichau and Stülke 2018). Inactivation of potassium uptake systems counteracts the increased susceptibility of *Lactococcus lactis* mutant unable to synthesize cdA, in agreement with a model linking ß-lactam susceptibility with impaired osmotic regulation (Pham et al. 2021). Nevertheless, the inactivation of cdA-metabolizing enzymes results in pleiotropic phenotypes, including variations in growth rate, transcriptomic perturbations, and morphology, which complicates interspecies comparisons. For instance, inactivation of GdpP (called Pde1) in *S. pneumoniae* is not associated with fitness defect and cell size are reduced in acapsulated strains only (Kobras et al. 2023), whereas electronic microscopy shows aberrant cell envelope ultrastructure in *S. aureus* (Corrigan et al. 2015, Sommer et al. 2021). Phenotypic variability needs to be linked to the evolution of the cdA signaling network. While the regulation of osmotic homeostasis is conserved, the precise molecular mechanisms have evolved, even in closely related species (Wang et al. 2022b, Schwedt et al. 2023, Turner et al. 2023, Wright and Bai 2023). This is probably the consequence of an ancient and essential regulatory mechanism that has had time to adapt to the specific environment and physiology of each species.

The core of the system is the coordinated regulation of osmolytes transporters at the transcriptional and post-translational levels. In GBS, ß-lactam tolerance of the *gdpP* mutant is recapitulated by the simultaneous inactivation of cdA-regulated osmolytes transporters, either repressed by BusR (BusAB) or by allosteric inhibition (KtrA, TrkA, and OpuCA). The activity of ß-lactams weakens the cell wall, causing an osmotic imbalance. Rebalancing involves exchanges of osmolytes in an ordered flow of potassium and zwitternionic molecules. Functional redundancy

ensures that the system remains functional in a variable environment, considering factors such as extracellular osmolyte concentration and physico-chemical characteristics (Stautz et al. 2021). Cda acts as a rheostat on these redundant transporters and the high concentration in the *gdpP* mutant locks osmolytes exchanges. The resulting reduction in turgor pressure has an impact on cell growth, probably through partial plasmolysis, as suggested by electronic microscopy. The advantage against the lytic activity of ß-lactams comes at a cost of a decreased ability to adapt to hyperosmotic environment. It is likely that the individual contribution of the transporters varies from one species to another (Wang et al. 2022b, Turner et al. 2023), depending on their physiological and environmental lifestyle, but that their simultaneous inhibition conservatively regulates ß-lactam tolerance or resistance.

A major difference between species is the cdA-dependent transcription mechanisms. In GBS, *L. lactis*, and *Clostridioides difficile*, the key transcriptional regulator is the BusR repressor (Romeo et al. 2003, Devaux et al. 2018, Bandera et al. 2021, Pham et al. 2021, Oberkampf et al. 2022). In addition to the conserved regulation of the *busAB* transporter genes, the BusR regulon includes the *amaP*-operon and the *pepY2* gene. Homologues of AmaP and related Asp23 proteins in *S. aureus* and *Bacillus subtilis* are involved in envelope homeostasis, either acting at the level of the cell wall or cell membranes (Muller et al. 2014, Tödter et al. 2017, Barros et al. 2019). Additionally, the membrane spanning PepY2 protein containing two PepSY ectodomains, originally predicted to inhibit extracellular proteases or glycosylases (Yeats et al. 2004), has homologues (TseB and CopB) recently characterized as part of the elongasome complex regulating PBP activity (Delisle et al. 2021, Lenoir et al. 2023). It is, thus likely that BusR integrates osmoregulation with envelope homeostasis. Turgor pressure exerts mechanical forces on cell envelopes, affecting cell growth, membrane tension, and cell wall remodeling (Rojas and Huang 2017). Membrane polarization and flow of cell-wall metabolite intermediates across membranes are critical for adjusting cellular activity to the osmolarity of the environment (Rojas et al. 2017). Further studies are necessary to define in which pathway AmaP/Asp23/GlsB and PepY2 are involved, without excluding a direct function in cell wall remodeling. Determining the dynamics of the response is also necessary. Especially, the *amaP* operon mediated ß-lactam susceptibility when BusR is inactivated but does not have a significant effect when WT cells are challenged with ß-lactams. This should be contextualized with the most significant effect observed upon potassium transporter inactivation, suggesting that BusR transcriptional regulation is a secondary response that restores a new equilibrium in turgor pressure.

Inactivation of *gdpP* has been proposed to be a first step in the evolution toward high-level ß-lactam resistance (Kobras et al. 2023). From an ethical point of view, the selection of ß-lactam-resistant GBS is prohibited by the scientific community, as is the introduction of a ß-lactamase gene, to prevent any risk of dissemination. In this study, we have first tested available mutants (Devaux et al. 2018) and extended the analysis to a random collection of insertional mutants, similarly generated in other laboratories (Hooven et al. 2016, Dammann et al. 2021) and as recently done in *S. pyogenes* (Zhu et al. 2022). Comprehensive screening by Tn-seq in *S. pyogenes* reveals the function of the ClpX chaperone and CcpA metabolic regulator in reduced ß-lactam susceptibility (Zhu et al. 2022). Our screen with individual mutants positively selected in similar conditions identified three main proteins or protein complex whose functions are cell-wall related but uncharacterized to date: the lysozyme-like GH25 hydrolase, the immunomodulatory Protein S with a peptidoglycan binding domain (Wierzbicki et al. 2019, Campeau et al. 2021), and the small RNA chaperone KhpAB, which regulates ß-lactam susceptibility in several species (Zheng et al. 2017, Olejniczak et al. 2022, Michaux et al. 2023). Patterns of secondary mutations in the insertional transposon mutants suggest functional links between the three, either as additive or compensatory mechanisms. Deciphering these functions will improve our understanding of cell wall synthesis and regulation and could provide clues as to the specificity of GBS, particularly the absence of any reported clinical resistance to date. Indeed, the most tolerant mutants identified in this study are unlikely to become fixed in natural populations due to their pleiotropic effects, including on virulence (Zheng et al. 2017, Wierzbicki et al. 2019, Campeau et al. 2021, Olejniczak et al. 2022). On the other hand, we cannot exclude at this stage the possibility of adaptive mechanisms similar to those observed to compensate for *gdpP* or *pbp* mutations in clinical isolates of related pathogens (Albarracin Orio et al. 2011, Gibson et al. 2022, Kobras et al. 2023).

Overall, characterization of the cdA-signaling network in GBS shows that ß-lactam tolerance is due to its function in coordinating osmotic pressure, a model that could be applied to related pathogens. In addition to cdA metabolism as a conserved mechanism of ß-lactams tolerance or reduced susceptibility, we investigated the distinctive features of GBS and identified cell wall-related mechanisms independent of PBP mutations that could pave the way for resistance.

Declaration of generative AI and AI-assisted technologies in the writing process

During the preparation of this work the authors used ChatGPT 3.5 to improve the readability and language of sections of the manuscript. After using this tool, the authors reviewed and edited the content as needed and take full responsibility for the content of the published article.

Acknowledgements

A.S. is the recipient of an AMR Master Student grant from Institut Pasteur.

Authors' contribution

Terry Brissac (Investigation, Validation), Cécile Guyonnet (Investigation), Aymane Sadouni (Investigation), Ariadna Hernández-Montoya (Investigation), Elise Jacquemet (Formal analysis), Rachel Legendre (Formal analysis), Odile Sismeiro (Investigation), Patrick Trieu-Cuot (Funding acquisition, Validation), Philippe Lanotte (Investigation, Supervision, Validation), Asmaa Tazi (Supervision, Validation) and Arnaud Firon (Conceptualization, Funding acquisition, Investigation, Supervision, Validation, Writing – original draft, Writing – review & editing)

Supplementary data

Supplementary data is available at *FEMSML Journal* online.

Conflict of interest: The authors declare no competing interests.

Funding

This study was supported by Fondation pour la Recherche Médicale (FRM—DEQ20181039599), and the National Laboratory of

Excellence program—Integrative Biology of Emerging Infectious Diseases (LabEx IBEID, ANR-10-LABX-62-IBEID).

Data availability

Raw sequencing reads and statistical analysis have been deposited in the Gene Expression Omnibus (https://www.ncbi.nlm.nih.gov/geo/) under GEO accession number GSE262190.

References

Albarracin Orio AG, Pinas GE, Cortes PR *et al.* Compensatory evolution of *pbp* mutations restores the fitness cost imposed by beta-lactam resistance in *Streptococcus pneumoniae*. *PLoS Pathog* 2011;**7**:e1002000.

Argudin MA, Roisin S, Nienhaus L *et al.* Genetic diversity among *Staphylococcus aureus* isolates showing oxacillin and/or cefoxitin resistance not linked to the presence of mec genes. *Antimicrob Agents Chemother* 2018;**62**:e00091–18.

Ba X, Kalmar L, Hadjirin NF *et al.* Truncation of GdpP mediates β-lactam resistance in clinical isolates of *Staphylococcus aureus*. *J Antimicrob Chemother* 2019;**74**:1182–91.

Bandera AM, Bartho J, Lammens K *et al.* BusR senses bipartite DNA binding motifs by a unique molecular ruler architecture. *Nucleic Acids Res* 2021;**49**:10166–77.

Barros EM, Martin MJ, Selleck EM *et al.* Daptomycin resistance and tolerance due to loss of function in *Staphylococcus aureus dsp1* and *asp23*. *Antimicrob Agents Chemother* 2019;**63**:e01542–01518.

Brauner A, Fridman O, Gefen O *et al.* Distinguishing between resistance, tolerance and persistence to antibiotic treatment. *Nat Rev Micro* 2016;**14**:320–30.

Campeau A, Uchiyama S, Sanchez C *et al.* The S protein of group B *Streptococcus* is a critical virulence determinant that impacts the cell surface virulome. *Front Microbiol* 2021;**12**:729308.

Cho H, Uehara T, Bernhardt TG. Beta-lactam antibiotics induce a lethal malfunctioning of the bacterial cell wall synthesis machinery. *Cell* 2014;**159**:1300–11.

Chochua S, Metcalf B, Li Z *et al.* Invasive group A streptococcal penicillin binding protein 2x variants associated with reduced susceptibility to beta-lactam antibiotics in the United States, 2015-2021. *Antimicrob Agents Chemother* 2022;**66**:e0080222.

Choi PH, Vu TMN, Pham HT *et al.* Structural and functional studies of pyruvate carboxylase regulation by cyclic di-AMP in lactic acid bacteria. *Proc Natl Acad Sci USA* 2017;**114**:E7226–35.

Global Burden of Disease Antimicrobial Resistance Collaborators. Global mortality associated with 33 bacterial pathogens in 2019: a systematic analysis for the Global Burden of Disease Study 2019. *Lancet* 2022;**400**:2221–48.

Commichau FM, Gibhardt J, Halbedel S *et al.* A delicate connection: c-di-AMP affects cell integrity by controlling osmolyte transport. *Trends Microbiol* 2018;**26**:175–85.

Commichau FM, Stülke J. Coping with an essential poison: a genetic suppressor analysis corroborates a key function of c-di-AMP in controlling potassium ion homeostasis in Gram-positive bacteria. *J Bacteriol* 2018;**200**:e00166–18.

Corrigan RM, Abbott JC, Burhenne H *et al.* c-di-AMP is a new second messenger in *Staphylococcus aureus* with a role in controlling cell size and envelope stress. *PLoS Pathog* 2011;**7**:e1002217.

Corrigan RM, Bellows LE, Wood A *et al.* ppGpp negatively impacts ribosome assembly affecting growth and antimicrobial tolerance in Gram-positive bacteria. *Proc Natl Acad Sci USA* 2016;**113**:E1710–1719.

Corrigan RM, Bowman L, Willis AR *et al.* Cross-talk between two nucleotide-signaling pathways in *Staphylococcus aureus*. *J Biol Chem* 2015;**290**:5826–39.

Covaleda-Cortes G, Mechaly A, Brissac T *et al.* The c-di-AMP-binding protein CbpB modulates the level of ppGpp alarmone in *Streptococcus agalactiae*. *FEBS J* 2023;**290**:2968–92.

Da Cunha V, Davies MR, Douarre PE *et al.* *Streptococcus agalactiae* clones infecting humans were selected and fixed through the extensive use of tetracycline. *Nat Commun* 2014;**5**:4544.

Dammann AN, Chamby AB, Catomeris AJ *et al.* Genome-wide fitness analysis of group B *Streptococcus* in human amniotic fluid reveals a transcription factor that controls multiple virulence traits. *PLoS Pathog* 2021;**17**:e1009116.

Delisle J, Cordier B, Audebert S *et al.* Characterization of TseB: a new actor in cell wall elongation in *Bacillus subtilis*. *Mol Microbiol* 2021;**116**:1099–112.

Devaux L, Sleiman D, Mazzuoli MV *et al.* Cyclic di-AMP regulation of osmotic homeostasis is essential in Group B *Streptococcus*. *PLoS Genet* 2018;**14**:e1007342.

Eagle H, Musselman AD. The rate of bactericidal action of penicillin in vitro as a function of its concentration, and its paradoxically reduced activity at high concentrations against certain organisms. *J Exp Med* 1948;**88**:99–131.

Firon A, Tazi A, Da Cunha V *et al.* The abi-domain protein Abx1 interacts with the CovS histidine kinase to control virulence gene expression in group B *Streptococcus*. *PLoS Pathog* 2013;**9**:e1003179.

Gefen O, Chekol B, Strahilevitz J *et al.* TDtest: easy detection of bacterial tolerance and persistence in clinical isolates by a modified disk-diffusion assay. *Sci Rep* 2017;**7**:41284.

Gibhardt J, Heidemann JL, Bremenkamp R *et al.* An extracytoplasmic protein and a moonlighting enzyme modulate synthesis of c-di-AMP in *Listeria monocytogenes*. *Environ Microbiol* 2020;**22**:2771–91.

Gibhardt J, Hoffmann G, Turdiev A *et al.* c-di-AMP assists osmoadaptation by regulating the *Listeria monocytogenes* potassium transporters KimA and KtrCD. *J Biol Chem* 2019;**294**:16020–33.

Gibson PS, Bexkens E, Zuber S *et al.* The acquisition of clinically relevant amoxicillin resistance in *Streptococcus pneumoniae* requires ordered horizontal gene transfer of four loci. *PLoS Pathog* 2022;**18**:e1010727.

Giulieri SG, Guerillot R, Kwong JC *et al.* Comprehensive genomic investigation of adaptive mutations driving the low-level oxacillin resistance phenotype in *Staphylococcus aureus*. *mBio* 2020;**11**:e02882–20.

Glaser P, Rusniok C, Buchrieser C *et al.* Genome sequence of *Streptococcus agalactiae*, a pathogen causing invasive neonatal disease. *Mol Microbiol* 2002;**45**:1499–513.

Gonçalves BP, Procter SR, Paul P *et al.* Group B *Streptococcus* infection during pregnancy and infancy: estimates of regional and global burden. *Lancet Glob Health* 2022;**10**:e807–19.

Guerillot R, Da Cunha V, Sauvage E *et al.* Modular evolution of TnGBSs, a new family of integrative and conjugative elements associating insertion sequence transposition, plasmid replication, and conjugation for their spreading. *J Bacteriol* 2013;**195**:1979–90.

Gundlach J, Herzberg C, Kaever V *et al.* Control of potassium homeostasis is an essential function of the second messenger cyclic di-AMP in *Bacillus subtilis*. *Sci Signal* 2017;**10**:eaal3011.

Hooven TA, Catomeris AJ, Akabas LH *et al.* The essential genome of *Streptococcus agalactiae*. *BMC Genomics* 2016;**17**:406.

Horn DL, Zabriskie JB, Austrian R *et al.* Why have group A streptococci remained susceptible to penicillin? Report on a symposium. *Clin Infect Dis* 1998;**26**:1341–5.

Kimura K, Nagano N, Arakawa Y. Classification of group B streptococci with reduced beta-lactam susceptibility (GBS-RBS) based

on the amino acid substitutions in PBPs. *J Antimicrob Chemother* 2015;**70**:1601–3.

Kobras CM, Monteith W, Somerville S *et al.* Loss of Pde1 function acts as an evolutionary gateway to penicillin resistance in *Streptococcus pneumoniae*. *Proc Natl Acad Sci USA* 2023;**120**:e2308029120.

Kotkova H, Cabrnochova M, Licha I *et al.* Evaluation of TD test for analysis of persistence or tolerance in clinical isolates of *Staphylococcus aureus*. *J Microbiol Methods* 2019;**167**:105705.

Krüger L, Herzberg C, Wicke D *et al.* A meet-up of two second messengers: the c-di-AMP receptor DarB controls (p)ppGpp synthesis in *Bacillus subtilis*. *Nat Commun* 2021;**12**:1210.

Krüger L, Herzberg C, Wicke D *et al.* Sustained control of pyruvate carboxylase by the essential second messenger cyclic di-AMP in *Bacillus subtilis*. *mBio* 2022;**13**:e0360221.

Lee AJ, Wang S, Meredith HR *et al.* Robust, linear correlations between growth rates and beta-lactam-mediated lysis rates. *Proc Natl Acad Sci USA* 2018;**115**:4069–74.

Lenoir C, Pelletier A, Manuse S *et al.* The morphogenic protein CopD controls the spatio-temporal dynamics of PBP1a and PBP2b in *Streptococcus pneumoniae*. *mBio* 2023;**14**:e0141123.

Lopatkin AJ, Stokes JM, Zheng EJ *et al.* Bacterial metabolic state more accurately predicts antibiotic lethality than growth rate. *Nat Microbiol* 2019;**4**:2109–17.

Love MI, Huber W, Anders S. Moderated estimation of fold change and dispersion for RNA-seq data with DESeq2. *Genome Biol* 2014;**15**:550.

Luo Y, Helmann JD. Analysis of the role of *Bacillus subtilis* sigma(M) in beta-lactam resistance reveals an essential role for c-di-AMP in peptidoglycan homeostasis. *Mol Microbiol* 2012;**83**:623–39.

Massa SM, Sharma AD, Siletti C *et al.* c-di-AMP accumulation impairs muropeptide synthesis in *Listeria monocytogenes*. *J Bacteriol* 2020;**202**:e00307–20.

Mazzuoli MV, Daunesse M, Varet H *et al.* The CovR regulatory network drives the evolution of group B *Streptococcus* virulence. *PLoS Genet* 2021;**17**:e1009761.

Metcalf BJ, Chochua S, Gertz RE *et al.* Short-read whole genome sequencing for determination of antimicrobial resistance mechanisms and capsular serotypes of current invasive *Streptococcus agalactiae* recovered in the USA. *Clin Microbiol Infect* 2017;**23**:574 e577–14.

Michaux C, Gerovac M, Hansen EE *et al.* Grad-seq analysis of *Enterococcus faecalis* and *Enterococcus faecium* provides a global view of RNA and protein complexes in these two opportunistic pathogens. *Microlife* 2023;**4**:uqac027.

Moscoso JA, Schramke H, Zhang Y *et al.* Binding of cyclic di-AMP to the *Staphylococcus aureus* sensor kinase KdpD occurs via the universal stress protein domain and downregulates the expression of the kdp potassium transporter. *J Bacteriol* 2016;**198**:98–110.

Muller M, Reiss S, Schluter R *et al.* Deletion of membrane-associated Asp23 leads to upregulation of cell wall stress genes in *Staphylococcus aureus*. *Mol Microbiol* 2014;**93**:1259–68.

Nelson JW, Sudarsan N, Furukawa K *et al.* Riboswitches in eubacteria sense the second messenger c-di-AMP. *Nat Chem Biol* 2013;**9**:834–9.

Nishimoto AT, Dao TH, Jia Q *et al.* Interspecies recombination, not de novo mutation, maintains virulence after beta-lactam resistance acquisition in *Streptococcus pneumoniae*. *Cell Rep* 2022;**41**:111835.

Nolan AC, Zeden MS, Kviatkovski I *et al.* Purine nucleosides interfere with c-di-AMP levels and act as adjuvants to re-sensitize MRSA to beta-lactam antibiotics. *mBio* 2022;**14**:e0247822.

Oberkampf M, Hamiot A, Altamirano-Silva P *et al.* c-di-AMP signaling is required for bile salt resistance, osmotolerance, and long-term host colonization by *Clostridioides difficile*. *Sci Signal* 2022;**15**:eabn8171.

Olejniczak M, Jiang X, Basczok MM *et al.* KH domain proteins: another family of bacterial RNA matchmakers?. *Mol Microbiol* 2022;**117**:10–19.

Paul P, Goncalves BP, Le Doare K *et al.* 20 million pregnant women with group B *Streptococcus* carriage: consequences, challenges, and opportunities for prevention. *Curr Opin Pediatr* 2023;**35**:223–230.

Peterson BN, Young MKM, Luo S *et al.* (p)ppGpp and c-di-AMP homeostasis is controlled by CbpB in *Listeria monocytogenes*. *mBio* 2020;**11**:e01625–20.

Pham HT, Nhiep NTH, Vu TNM *et al.* Enhanced uptake of potassium or glycine betaine or export of cyclic-di-AMP restores osmoresistance in a high cyclic-di-AMP *Lactococcus lactis* mutant. *PLoS Genet* 2018;**14**:e1007574.

Pham HT, Shi W, Xiang Y *et al.* Cyclic di-AMP oversight of counter-ion osmolyte pools impacts intrinsic cefuroxime resistance in *Lactococcus lactis*. *mBio* 2021;**12**:e00324–21.

Rao F, See RY, Zhang D *et al.* YybT is a signaling protein that contains a cyclic dinucleotide phosphodiesterase domain and a GGDEF domain with ATPase activity. *J Biol Chem* 2010;**285**:473–82.

Rismondo J, Gibhardt J, Rosenberg J *et al.* Phenotypes associated with the essential diadenylate cyclase CdaA and its potential regulator CdaR in the Human pathogen *Listeria monocytogenes*. *J Bacteriol* 2016;**198**:416–26.

Rojas ER, Huang KC, Theriot JA. Homeostatic cell growth is accomplished mechanically through membrane tension inhibition of cell-wall synthesis. *Cell Syst* 2017;**5**:578–590.e6.e576.

Rojas ER, Huang KC. Regulation of microbial growth by turgor pressure. *Curr Opin Microbiol* 2018;**42**:62–70.

Romeo Y, Obis D, Bouvier J *et al.* Osmoregulation in *Lactococcus lactis*: busR, a transcriptional repressor of the glycine betaine uptake system BusA. *Mol Microbiol* 2003;**47**:1135–47.

Salzer A, Wolz C. Role of (p)ppGpp in antibiotic resistance, tolerance, persistence and survival in Firmicutes. *Microlife* 2023;**4**:uqad009.

Schwedt I, Wang M, Gibhardt J *et al.* Cyclic di-AMP, a multifaceted regulator of central metabolism and osmolyte homeostasis in *Listeria monocytogenes*. *Microlife* 2023;**4**:uqad005.

Seki T, Kimura K, Reid ME *et al.* High isolation rate of MDR group B streptococci with reduced penicillin susceptibility in Japan. *J Antimicrob Chemother* 2015;**70**:2725–8.

Sommer A, Fuchs S, Layer F *et al.* Mutations in the *gdpP* gene are a clinically relevant mechanism for beta-lactam resistance in meticillin-resistant *Staphylococcus aureus* lacking mec determinants. *Microb Genom* 2021;**7**:000623.

Stautz J, Hellmich Y, Fuss MF *et al.* Molecular mechanisms for bacterial potassium homeostasis. *J Mol Biol* 2021;**433**:166968.

Stülke J, Krüger L. Cyclic di-AMP signaling in bacteria. *Annu Rev Microbiol* 2020;**74**:159–79.

Sureka K, Choi PH, Precit M *et al.* The cyclic dinucleotide c-di-AMP is an allosteric regulator of metabolic enzyme function. *Cell* 2014;**158**:1389–401.

Tödter D, Gunka K, Stülke J. The highly conserved Asp23 family protein YqhY plays a role in lipid biosynthesis in *Bacillus subtilis*. *Front Microbiol* 2017;**8**:883.

Tosi T, Hoshiga F, Millership C *et al.* Inhibition of the *Staphylococcus aureus* c-di-AMP cyclase DacA by direct interaction with the phosphoglucosamine mutase GlmM. *PLoS Pathog* 2019;**15**:e1007537.

Tuomanen E, Cozens R, Tosch W *et al.* The rate of killing of *Escherichia coli* by beta-lactam antibiotics is strictly proportional to the rate of bacterial growth. *J Gen Microbiol* 1986;**132**:1297–304.

Turner MS, Xiang Y, Liang ZX *et al.* Cyclic-di-AMP signalling in lactic acid bacteria. *FEMS Microbiol Rev* 2023;**47**:fuad025.

Wang M, Buist G, van Dijl JM. *Staphylococcus aureus* cell wall maintenance—the multifaceted roles of peptidoglycan hydrolases in bacterial growth, fitness, and virulence. *FEMS Microbiol Rev* 2022a;**46**:fuac025.

Wang M, Wamp S, Gibhardt J *et al.* Adaptation of *Listeria monocytogenes* to perturbation of c-di-AMP metabolism underpins its role in osmoadaptation and identifies a fosfomycin uptake system. *Environ Microbiol* 2022b;**24**:4466–88.

Whiteley AT, Garelis NE, Peterson BN *et al.* c-di-AMP modulates *Listeria monocytogenes* central metabolism to regulate growth, antibiotic resistance and osmoregulation. *Mol Microbiol* 2017;**104**:212–33.

Wierzbicki IH, Campeau A, Dehaini D *et al.* Group A streptococcal S protein utilizes red blood cells as immune camouflage and is a critical determinant for immune evasion. *Cell Rep* 2019;**29**:2979–89.

Wright MJ, Bai G. Bacterial second messenger cyclic di-AMP in streptococci. *Mol Microbiol* 2023;**120**:791–804.

Yeats C, Rawlings ND, Bateman A. The PepSY domain: a regulator of peptidase activity in the microbial environment?. *Trends Biochem Sci* 2004;**29**:169–72.

Zheng JJ, Perez AJ, Tsui HT *et al.* Absence of the KhpA and KhpB (JAG/EloR) RNA-binding proteins suppresses the requirement for PBP2b by overproduction of FtsA in *Streptococcus pneumoniae* D39. *Mol Microbiol* 2017;**106**:793–814.

Zhu L, Eraso JM, Mangham RE *et al.* Genome-wide transposon mutagenesis screens identify group A *Streptococcus* genes affecting susceptibility to beta-lactam antibiotics. *J Bacteriol* 2022;**204**:e0028722.

Zhu Y, Pham TH, Nhiep TH *et al.* Cyclic-di-AMP synthesis by the diadenylate cyclase CdaA is modulated by the peptidoglycan biosynthesis enzyme GlmM in *Lactococcus lactis*. *Mol Microbiol* 2016;**99**:1015–27.

Received 6 May 2024; **revised** 3 June 2024; **accepted** 11 June 2024